

The cD galaxy Hydra A: evidence for cooling-flow driven star formation in a fast rotating central disk^{*}

J. Melnick, Gopal-Krishna^{**}, and R. Terlevich^{***}

European Southern Observatory, Casilla 19001, Santiago-19, Chile

Received 7 April 1995 / Accepted 5 April 1996

Abstract. For the nearby powerful radio galaxy Hydra A, which is thought to lie at the centre of a massive cooling flow, we report the results of optical spectroscopy plus high-resolution H α and 2.2 μ imaging.

We detected strong nuclear emission lines with line ratios characteristic of LINERs. The nuclear emission region is resolved and the tilt of the emission lines indicates that they originate in a gaseous disk-like structure with a rotational velocity of $\sim 300 \text{ km s}^{-1}$.

We find extended Balmer absorption lines of strengths characteristic of O-B type stars in the spectrum of the central region bluewards of the 4000 \AA break. The Balmer lines are also tilted indicating that the O-B stars are co-rotating with the gas. This is in contrast with the older stellar population which show no evidence for rotation. Our result indicates a close link between the young stars and the emitting gas. We suggest that the material needed for the formation of these young stars and the gaseous disk may be deposited near the centre by the cooling flow.

We examine the physical conditions within the nebula together with possible sources of energy input by confronting the observed emission-line ratios with predictions of models with different excitation mechanisms and conclude that photoionization by a combination of hot stars and X-ray is able to explain the observed line ratios.

Key words: galaxies: cooling flows – radio continuum: galaxies – galaxies: jets – galaxies: kinematics and dynamics – galaxies: stellar content – galaxies: individual: Hydra A

1. Introduction

The discovery of an extremely low-excitation (LINER type) optical spectrum in the powerful double radio source 1411-192

^{*} Based on observations collected at the European Southern Observatory.

^{**} Permanent address: National Centre for Radio Astrophysics, Tata Institute of Fundamental Research, Poona Univ. Campus, Pune-411007, India

^{***} Permanent address: Royal Greenwich Observatory, Madingley Road, Cambridge CB3 0EZ, England

($z = 0.477$) first provoked our interest in this intriguing class of radio sources (Gopal-Krishna et al., 1992). We noted in that paper that the nearby radio galaxy Hydra A is a prime specimen of the class characterized by the combination of high radio luminosity with ultra-steep spectrum *and* a LINER type soft optical emission-line spectrum. In the present paper we endeavour to examine the nature of this well known (albeit not so well studied) powerful radio source by employing new optical and near-IR observations.

1.1. Hydra A (3C218, PKS0915 – 118): basic properties

Having a bright parent galaxy ($m_B = 14.58$, Sandage, 1973), Hydra A was one of the first extragalactic radio sources to be identified (Mathews, Morgan & Schmidt, 1964). Located at a projected separation of 13 *arcmin* from the centre, the cD2 galaxy identified with Hydra A is the dominant member of the poor cluster Abell 780 (Bautz-Morgan type I, Abell richness class 0, see Sandage & Hardy 1973). The Einstein observatory revealed it to be a very strong X-ray source with $L_X \sim 2 \times 10^{44} \text{ erg s}^{-1}$. The X-ray emission is well modeled in terms of thermal plasma at a temperature of 4.5 keV with a core radius of $\sim 100 \text{ kpc}$, a central hydrogen density, $n_H \sim 0.005 \text{ cm}^{-3}$, and an estimated cooling flow rate of $\sim 270 M_\odot \text{ yr}^{-1}$ (David et al., 1990; all estimates have been scaled to $H_0 = 75 \text{ km s}^{-1} \text{ Mpc}^{-1}$).

The redshift of Hydra A ($z = 0.0545$) places it at a distance of 215 Mpc yielding a scale of $1'' = 0.95 \text{ kpc}$. Thus, the overall radio size as seen on the VLA maps is $\sim 450 \text{ kpc}$ (Taylor et al., 1990; Baum et al., 1988). The maps also show that the two radio jets are curved, display ‘S’ symmetry, and flare abruptly at a distance of about 5 kpc from the nucleus. The nucleus has a flat radio spectrum (Tabara et al., 1990) and its position measured to an accuracy of $\sim 0.1''$ from the 4.6 GHz VLA map (Taylor et al., 1990) is:

R.A. (1950): $09^h 15^m 41.19^s$;
Dec.(1950): $-11^\circ 53' 05.0''$

Within the local Universe ($z \leq 0.1$), Hydra A is superseded in radio power only by Cygnus-A. At $z \sim 0.05$ both galaxies are *at least* an order-of-magnitude more luminous than the Fanaroff-Riley break which occurs at $P_{1\text{GHz}} \sim 10^{25.5} \text{ W Hz}^{-1}$ (Fanaroff & Riley, 1974). Intriguingly Hydra A exhibits an edge-darkened

radio structure characteristic of weaker radio galaxies (Ekers & Simkin, 1983; Baum et al., 1988; Taylor et al., 1990).

Hydra A is one of the few known extragalactic radio sources having a large integrated rotation measure ($RM \geq 1000 \text{ rad.m}^{-2}$), another property it shares with Cygnus-A also located inside a cooling flow cluster (Kato et al., 1987). From VLA polarimetric observations the rotation measure across the radio lobes is found to be distinctly asymmetric about the nucleus. By modeling these data it has been inferred that the radio axis is inclined from the line-of-sight by $\sim 48^\circ$ and that the northern lobe lies on the near side from us (Taylor & Perley, 1993).

Around the radio nucleus, Baum et al.(1988) have detected an extended emission line region (EELR) with a total $H\alpha$ luminosity of $\sim 8 \times 10^{40} \text{ erg s}^{-1}$. The EELR occupies the gap between the two radio lobes and exhibits a prominent curved $H\alpha$ filament to the north. According to these authors the inner part of the EELR consists of a flattened elliptical nebula of size $\sim 6''$ roughly centered on the nucleus whose minor axis coincides with the rotation axis at $PA \sim 29^\circ$, as determined by Simkin (1979). On the other hand there is no evidence for rotation of the stellar component, the nominal rotation velocity being $13 \pm 18 \text{ km s}^{-1}$ (Heckman et al., 1985). In the classification scheme of Heckman et al.(1989), Hydra A is a class-II cooling flow nebula. Such nebulae are characterized by high $H\alpha$ and X-ray luminosities and relatively weak [NII] and [SII] lines, but rather strong [OI]6300 emission characteristic of LINERs. The excitation mechanism of these systems is not well understood and is somewhat controversial (see e.g. Crawford & Fabian 1992 henceforth CF, and references therein). In a recent work McNamara (1995) finds a central disk with colours consistent with a burst of star formation of $\sim 10^{8-9} M_\odot$. About 30 to 40% of the observed U light is due to these young stars. Furthermore, Hansen et al. (1995) detected Balmer absorptions in the central disk. They concluded that the absorptions were compatible with a recent burst of star formation with age $\sim 10^7 \text{ yr}$ and mass $10^{8-9} M_\odot$.

In order to examine these issues, we have carried out optical/near-IR imaging as well as long slit optical spectroscopy of this source, the results of which are reported here.

2. Observations

2.1. High resolution imaging

$H\alpha$ images of Hydra A under excellent seeing conditions were obtained with SUSI at the New Technology Telescope on La Silla in January, 1992. The data were kindly secured by Dr. Bo Reipurth who observed the galaxy for 15 minutes through a 64 \AA -wide filter centered at $\lambda=6939 \text{ \AA}$. The detector was a Tek1024 CCD (ESO#25) with 24μ pixels corresponding to $0.13''$ giving a total field of view of $2.2' \times 2.2'$. The central $30'' \times 30''$ of the image are shown in Fig. 1. Since no off-band image was taken, this image shows the line plus continuum emission. Contour plots of the pure line emission can be found

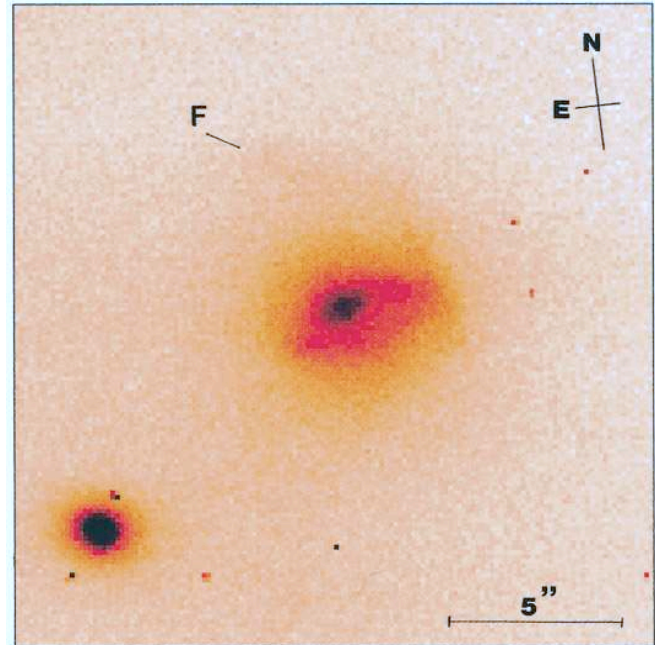


Fig. 1. Narrow-band ($H\alpha$ plus continuum) image of Hydra A (seeing $0.6''$). From the western side an extension (marked 'F') seems to start to the northeast and then bend eastward approaching the radio jet position (Sect. 4.5). The object in the lower left corner is a galaxy which is most probably not interacting with Hydra A (Sect. 3.5).

in Hansen et al.(1995). The size of the seeing disk measured on this image is $0.61''$ (FWHM).

A K-band image of the galaxy was obtained at our request by Dr. Patrice Bouchet with IRAC2b on the 2.2m telescope at La Silla. The total integration time was 30 minutes using objective C that gives a pixel size of $0.52''$. In this configuration the 256^2 NICMOS3 array covers slightly more than one square arc minute. The seeing measured in these images is $1.3''$. The central portion of the K-band image is shown in Fig. 2.

2.2. Spectroscopy

Grism spectroscopy at low and intermediate resolution was carried out with EFOSC1 on the 3.6m telescope at La Silla in 1992, February. All observations were obtained under moderate seeing conditions ($\sim 1.5''$) using a $1.5''$ slit at two position angles: along the inner axis of the radio source ($PA=12^\circ$) and perpendicular to it ($PA=102^\circ$). Only low resolution spectra were obtained at $PA=12^\circ$. The Grisms used were B150 ($3740 \text{ \AA}-5450 \text{ \AA}$; 3.3 \AA/pix), R150 ($6870 \text{ \AA}-8560 \text{ \AA}$; 3.3 \AA/pix), and R300 ($5940 \text{ \AA}-9770 \text{ \AA}$; 6.3 \AA/pix). For all spectra the slit was centered on the nucleus using R band images taken immediately before each exposure. Thus, we estimate that the spectra are centered on the nucleus to an accuracy better than $0.4''$. The integration times were 30min for B150 and R150, $3 \times 30 \text{ min}$ for R300 at $PA=102^\circ$, and 30min for R300 at $PA=12^\circ$.

The spectra were flux calibrated using the standard star W485a observed on the same night with the same instrumen-

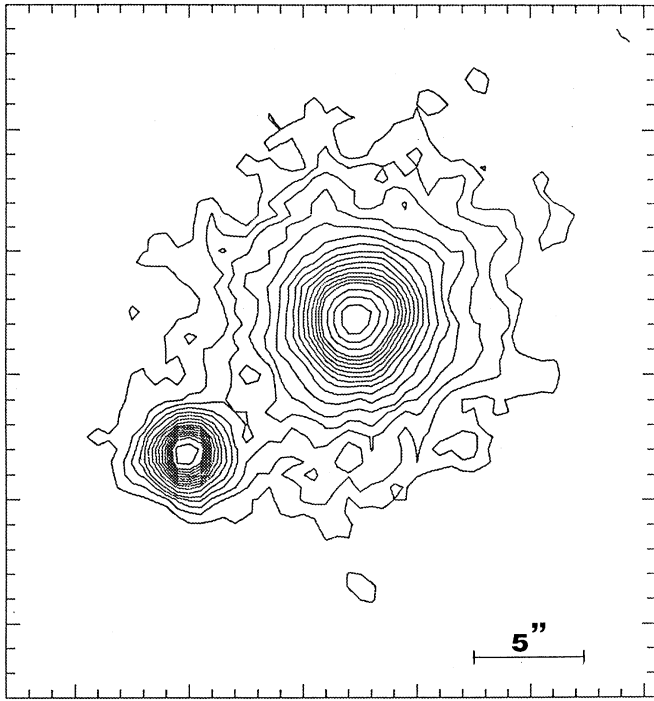


Fig. 2. K-band (2.2μ) isophotes of Hydra A (seeing $1.3''$). North is on the top and east is to the left. The contour interval is 1 unit (on arbitrary scale) for the first 4 contours, 1.5 units for the next 11 contours and 3 units for the innermost 3 contours. The lack of any global distortion of the contours argues for the absence of major tidal interaction between Hydra A and the neighbouring galaxy visible to the southeast.

tal configuration, and at very nearly the same airmass as Hydra A. All reductions were done within context LONG in MIDAS which was also used to subtract the sky. This was done by fitting each column independently over 20 pixels ($12''$) at either side and $25''$ away from the nucleus, well outside the halo visible on the R exposures. Thus we estimate that the contamination of the sky spectrum by light from the galaxy halo is negligible. The wavelength calibration was done using the 2-pass row-by-row algorithm of LONG which ensures that the same set of He-Ar lines is used to calibrate each row. Thus, the residual line distortions in the reduced intermediate resolution spectra are less than 0.1\AA peak-to-peak.

The resulting flux calibrated, sky subtracted spectra are shown in Figs. 3 and 4. Fig. 3 shows the intermediate resolution spectra ($PA=102^\circ$) where the emission lines are seen to be markedly tilted, while some absorption lines appear to be tilted and others not. An important feature to note is that the emission lines are not only tilted, but are also broader near the nucleus of the galaxy.

Fig. 4 shows the low dispersion spectra at the two position angles. While the emission lines are clearly seen to be tilted at $PA=102^\circ$, they are flat at $PA=12^\circ$. At a larger distance from the nucleus towards the North, however, the lines are bent towards lower velocities.

3. Data analysis

3.1. Gas kinematics

Our $H\alpha$ image shows a central disk of elliptical shape containing a bright nucleus. Our spectra show this region to be in rapid rotation. The “rotation curve” at $PA = 102^\circ$ shows in fact that the entire disk is rotating with a total amplitude of more than 500 km s^{-1} which is considerably larger than that reported by Heckman et al.(1985). The rotation curve is plotted in Fig. 5 where the zero point of the velocity scale has been set at the point of maximum light which coincides with the position of the nucleus seen in Fig. 1.

The sharp decrease in the rotation velocity at 2.5 kpc East of the nucleus and the slight increase in velocity at about 3.5 kpc from the nucleus on the western side are both real and coincide with the opposite edges of the disk.

Additional information about the kinematics of the ionized gas comes from the observed line widths. Fig. 6 shows a plot of the $H\alpha$ line-profile width corrected for instrumental broadening as a function of radius measured along the slit at $PA = 102^\circ$. We used the multi-component Gaussian fitting option of the context ALICE in MIDAS to measure the line widths by simultaneously fitting $H\alpha$ and the two adjacent [NII] lines. The error bars represent the combined effect of the fitting errors and the uncertainty in the instrumental PSF. The lines are seen to be resolved indicating an average (turbulent) velocity dispersion of $\sigma \sim 80\text{ km s}^{-1}$ which increases markedly towards the nucleus where it reaches $\sigma \sim 120\text{ km s}^{-1}$. Close inspection of the 2-D spectrum (Fig. 3a and b) suggests that the line broadening near the nucleus may in fact be due to an unresolved steepening of the rotation curve, but on the basis of our data alone we conclude that the gas becomes increasingly more turbulent towards the nucleus.

In the spectrum at $PA = 12^\circ$ we find no evidence for rotation (Fig. 4a), consistent with the results of Simkin (1979) and Hansen et al.(1995). In the northern part of the nebula, however, we do notice a significant tilt of the emission lines. The velocity difference between the $H\alpha$ peak (nucleus) and the northern edge (about $6''$ away), which coincides with the filament marked F on the $H\alpha$ image (Fig. 1), is $+170 \pm 15\text{ km s}^{-1}$. Thus the filament is blue-shifted relative to the nucleus. Hansen et al.(1995) also find that this filament is blue shifted relative to the nucleus, but they quote without errors a velocity difference of only 110 kms. We do not know if the difference is consistent with the errors (which are large because the filament is very faint) or due to other factors like a different position of the slit. For the purpose of our analysis, however, the important thing is that the filament is blue shifted relative to the nucleus. We will return to this point in Sect. 4.5 .

3.2. Stellar kinematics

Heckman et al.(1985) found that Hydra A has negligible rotation ($13 \pm 18\text{ km s}^{-1}$), but their observations are limited to the spectral range 4200 to 5700 \AA in the Hydra A rest frame and thus do not include the higher Balmer series lines. On the other hand,

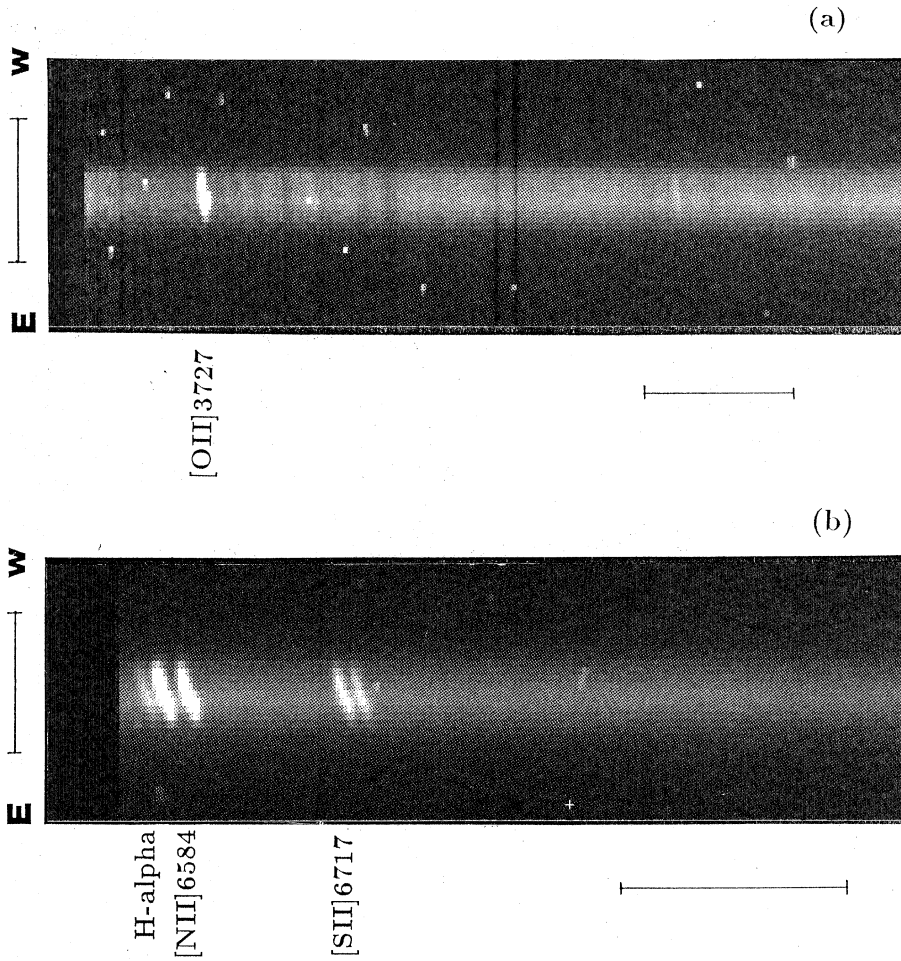


Fig. 3a and b. Medium-resolution blue and red spectra taken with a $1.5''$ slit at $PA = 102^\circ$ and centered at the position of the $H\alpha$ peak. The vertical and horizontal bars correspond to $10''$ and 200\AA , respectively. All emission lines are clearly tilted implying a rapid rotation of the disk and of the spiral pattern embedded in it (Sect. 3.1). There is a hint of a similar tilt in the Balmer absorption lines seen just longward of the $[OII]3727$ emission (Sect. 3.2). In contrast, the H and K absorption lines seem to show no tilt implying negligible rotation of the main stellar body of the galaxy.

Ekers & Simkin (1983) report very fast rotation of stars in the central 20 kpc of the galaxy. In fact, their H and K absorption-line data appears to show a tilt of about 350 km s^{-1} within 5 kpc from the nucleus along $PA \sim 115^\circ$, and a larger, very sharp drop beyond 5 kpc East of the center. The S/N of their photographic spectra, however, are rather low and since even their emission line rotation curves are only partly confirmed by our substantially higher quality observations, we shall examine the properties of the stellar component solely on the basis of our own data.

Fig. 7 shows our blue spectrum of the central region averaged over 5 kpc. The continuum is much bluer than that of a typical giant elliptical galaxy; normalized to the visual continuum (at 5000\AA) the blue continuum (3500\AA) is ~ 6 times stronger. This blue excess of the disk of Hydra A, also inferred previously from multi-colour photometry (e.g., Hansen 1989; Smith & Heckman 1989; McNamara 1995), is particularly interesting in conjunction with its rich absorption-line spectrum. In addition to strong CaII, Mgb, and G band, the spectrum shows strong Balmer absorption lines bluewards of the 4000\AA break. The lower lines of this series: $H\delta$, $H\gamma$, and $H\beta$ are not seen because they are filled-in by the nebular emission. In the case of Hydra A the continuum appears to be even bluer than that of E+A galaxies (Dressler and Gunn, 1983). It resembles the

blue spectrum of some central cluster galaxies (Crawford & Fabian 1993) and looks almost indistinguishable from that of NGC 1275 (compare Fig. 7 of this paper with Fig. 2 of Crawford & Fabian 1993).

Unfortunately our data lack the resolution and S/N to allow a detailed study of the stellar kinematics. Nonetheless, visual inspection of the blue part of the spectrum in two dimensions (Fig. 3) suggests that the Balmer absorption lines are tilted in the same sense as the nebular emission lines, whereas the lines typical of the older stellar population (CaII, G, Mgb) show no rotation. This impression is confirmed by the comparison of the extractions of opposite sides of the nucleus. The upper spectrum of Fig. 8 corresponds to a 3 pixel extraction to the West of the nucleus while the bottom spectrum corresponds to the 3 pixels immediately to the East of the nucleus. The two nuclear increments have not been included. Clearly the high order Balmer lines have a displacement similar to that of $[OII]\lambda 3727\text{\AA}$ while the H & K CaII lines show no displacement. Measurements of the rotation in the individual lines using multi-component Gaussian fits indicate little or no rotation in H and K, and a tilt of $450 \pm 130 \text{ km s}^{-1}$ in the central 3kpc for the higher Balmer absorption series ($\lambda\lambda 3889, 3835, \text{ and } 3798 \text{\AA}$). This is in remarkably good agreement with the gas kinematics in the same region (Sect. 3.1). Also, Hansen et al. (1995) find a difference

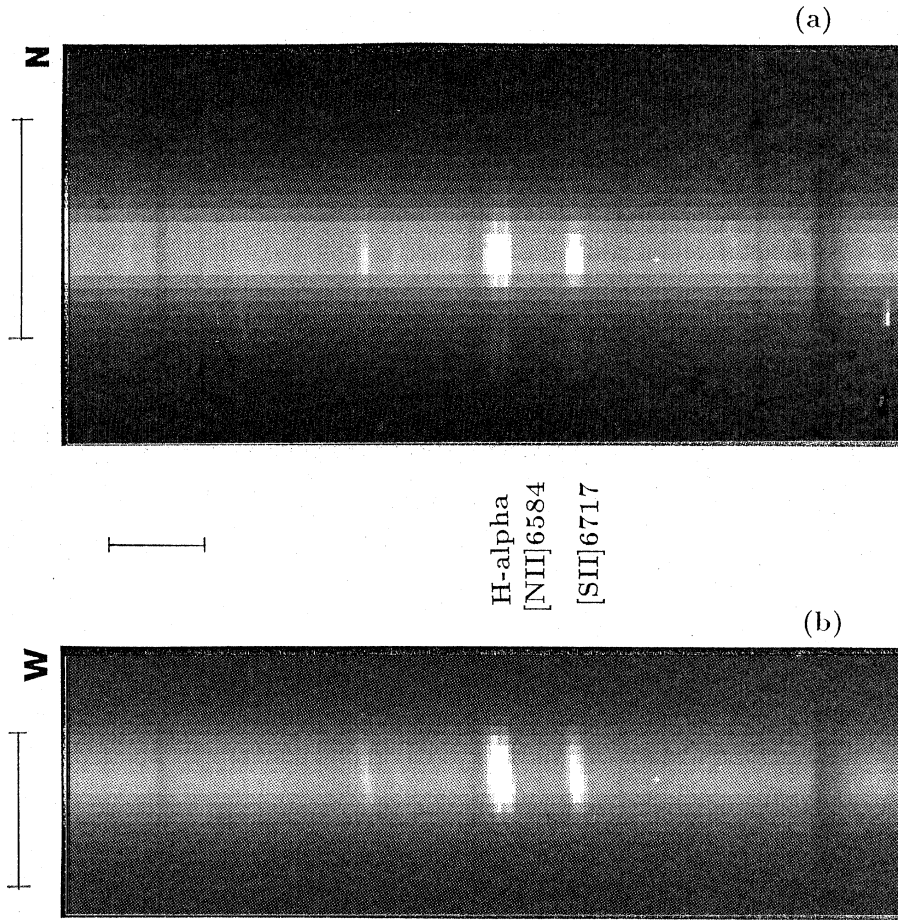


Fig. 4a and b. Low-resolution red spectra taken with slits oriented at PA = 12° and 102°, respectively, and centered on the H α peak. The vertical and horizontal bars correspond to 10'' and 200Å, respectively. The tilt of the emission lines is only seen at PA = 102° consistent with the rotation axis of the disk being close to the radio axis (PA ~ 20°; Sect. 3.1).

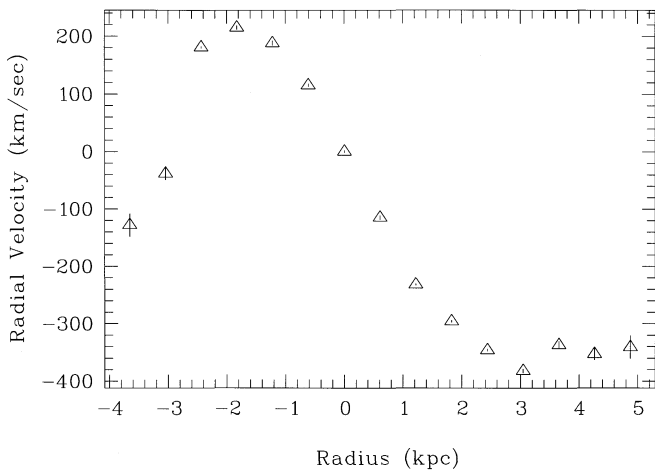


Fig. 5. Radial velocity measured along the slit centered at the H α peak and along PA = 102°. Note the large total velocity amplitude along the disk, which exceeds 500km s⁻¹ even without accounting for the inclination of the disk to the line-of-sight.

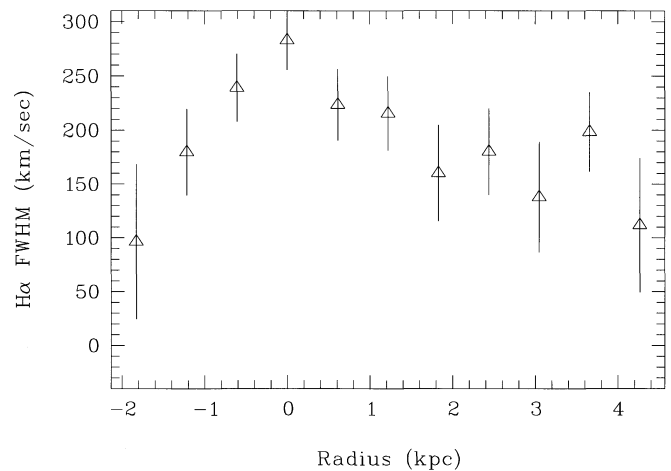


Fig. 6. Intrinsic width of the H α line measured along PA = 102°. East increases to the left.

of 300 km s⁻¹ between the radial velocity of Hydra A measured from the Balmer lines and that measured from the other absorption lines

Thus, taken together, the observations of the stellar composition and kinematics, and the colour of the disk component

(McNamara 1995) strongly point at recent star-formation activity in the center of Hydra A probably associated with the infall of gas in the form of a cooling flow (Sect. 4). Ionized gas and young stars seem to have similar disk-like kinematics while the old population seems to rotate slowly and be mainly pressure supported.

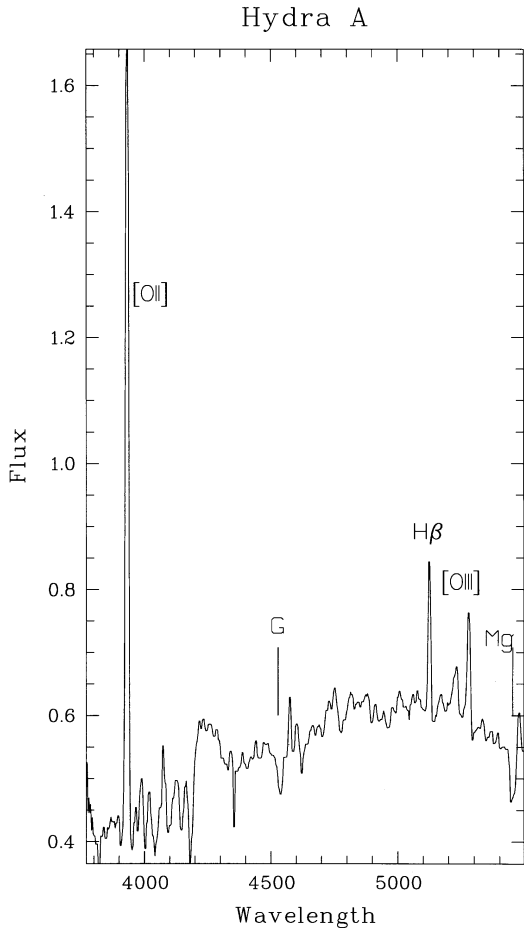


Fig. 7. Intermediate-resolution spectrum taken with the slit at PA = 102° . It shows the average over the central 5 kpc. Just longward of the bright [OII]3727 emission line one notices prominent Balmer absorption lines. The continuum is much bluer than that of typical nearby massive elliptical galaxies.

3.3. Emission line ratios

Our measurements yield the relative strengths of several important diagnostic lines as a function of distance from the nucleus along PA = 102° (see Table 1). The uncertainties vary widely according to the difficulty encountered in fitting the continuum. This was particularly difficult for $H\gamma$ and [OIII] λ 4363Å which are weak and flanked by absorption features, and for [NI] λ 5200 which lies at the edge of the spectrum very close to the Mg β absorption band.

The possible detection of the temperature sensitive line [OIII] λ 4363Å is particularly important. If real, it would allow placing very stringent constraints on the possible mechanisms for the excitation of the gas. Unfortunately, the line is very weak, and lies in a particularly difficult part of the spectrum. In order to define the continuum level and to measure its strength we have used multiple Gaussian to fit [OIII] and $H\gamma$ simultaneously forcing the widths to be the same and the positions to correspond to the redshifted laboratory wavelengths of the two lines. In order to improve the S/N two consecutive rows of pixels were

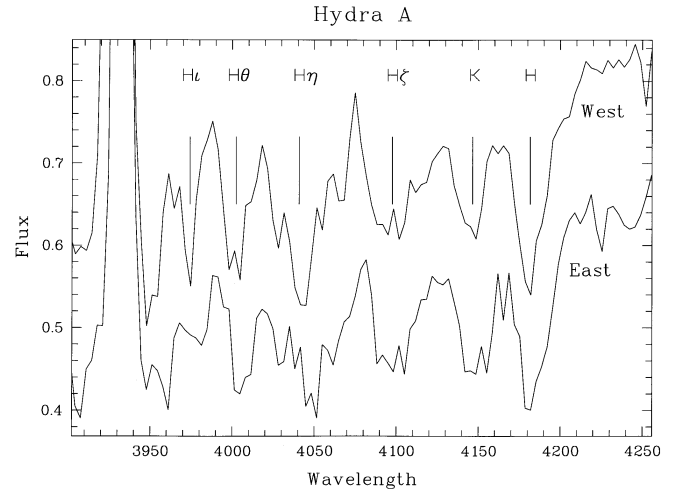


Fig. 8. Comparison of the blue spectra to the West and to the East of the nucleus obtained averaging 3 rows of pixels on either side, excluding the central 2 rows. The [OII]3727 emission and the high Balmer series absorptions are shifted while no shift is seen in the CaII H and K lines.

averaged for each Gaussian fitting. The rather large deduced intensity ratio, [OIII] λ 4363/ $H\gamma$ \sim 0.4, raises some doubts about the reality of the Oxygen line. In fact, a close inspection of the 2-D spectrum shows the feature to be somewhat broader and perhaps less tilted than $H\gamma$, but near the nucleus the line appears to be real (Fig. 3). We conclude that the detection of [OIII] λ 4363 is only tentative, and that no inferences about the physical conditions of the gas should be made based on this uncertain detection.

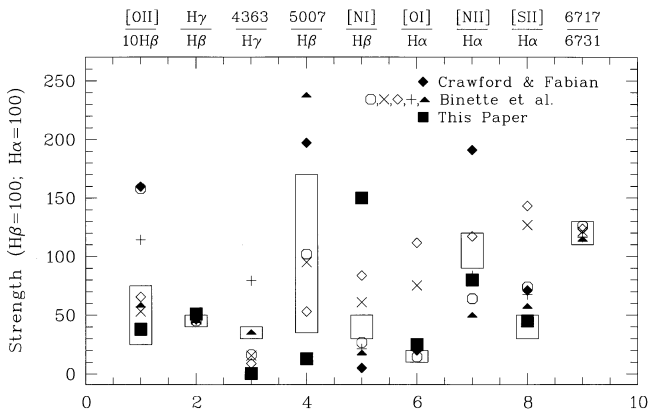
The line ratios given in Table 1 have not been corrected for underlying absorption of the Balmer lines which, as we saw in the previous section, is particularly strong in this object. In order to apply these corrections to a first order we have assumed that reddening is negligible (Hansen et al. 1995), and that the equivalent widths of the underlying Balmer absorption features ($H\beta$, $H\gamma$, and $H\delta$) are equal. Using the theoretical Case B recombination ratios ($H\gamma/H\beta = 0.46$ and $H\delta/H\beta = 0.25$) we then obtain an absorption equivalent width of $\sim 2\text{\AA}$ for the underlying absorption lines. This implies that some of the line ratios in Table 1 must be reduced by $\sim 30\%$ to correct for the effect of absorption in $H\beta$. The strength of $H\gamma$ is underestimated by a factor of 1.75 but the ratio of $H\gamma$ to $H\beta$ remains virtually unchanged. These corrections have been incorporated in Fig. 9 where the line ratios are compared with predictions of various models.

The strengths of the red lines are measured relative to $H\alpha$ which is little affected by underlying absorption. [OI] λ 6300Å was measured in the low dispersion spectrum relative to the [SII] doublet and then scaled to $H\alpha$ using the intensities measured on the intermediate dispersion spectrum. Note that the measured intensity of the [OI] λ 6300Å line is rather uncertain owing to its location near an atmospheric band.

There is a systematic gradient in the excitation level towards the nucleus. The [OII]/[OIII] ratio approaches a minimum at the

Table 1. Observed emission line ratios as a function of radius (PA = 102 degrees)

Radius (kpc)	[OII]/H β 3727	H γ /H β	[OIII]/H β 4959+5007	[NI]/H β 5200	[OI]/H α 6300	[NII]/H α 6584	[SII]/H α 6717
-1.2 (E)	7.2	*	0.87	*	0.2	1.06	0.45
-0.6	6.2	0.5	1.38	0.3	0.1	1.12	0.44
0	7.4	0.4	1.65	0.4	0.2	1.2	0.48
0.6	7.0	0.4	1.06	0.4	0.1	1.18	0.46
1.2	4.5	0.5	0.77	0.5	0.1	1.13	0.47
1.7	3.7	0.5	0.47	*	0.2	1.03	0.42
2.3	3.4	0.4	0.47	0.3	0.1	0.93	0.33
2.9 (W)	2.9	*	0.36	*	0.1	0.98	0.36

**Fig. 9.** Comparison of several diagnostic emission-line ratios with predictions of different theoretical models (Sect. 4.1). The rectangular boxes illustrate the ranges of the line ratios observed across the nebula through the slit at PA = 102°. The Balmer line intensities have been corrected for the underlying absorption.

position of the nucleus and drops gradually towards the West but sharply towards the East. The [OIII]/H β ratio peaks at the nucleus, too, but drops symmetrically on either side. The observed [SII] doublet ratios indicate densities of order 200 cm^{-3} .

3.4. Stellar populations

The combination of strong high Balmer series absorption lines and absence of continuum drop across $\lambda 3700 - 3800\text{\AA}$ strongly suggests that the blue continuum is due to a young burst of star formation dominated by O-B stars capable of ionizing the gas (Hansen et al. 1995, Crawford & Fabian 1993; Bica et al. 1994).

Our motivation for taking a long integration with the R300 grism at PA=102° was to investigate possible changes in the stellar populations in the core of the galaxy as revealed by the strength of the CaII triplet near $\lambda 8500\text{\AA}$ (Terlevich et al., 1990; Jones et al., 1984). No gradient was detected. This is also the case for the blue spectra where we detect no gradients in the strengths of the absorption lines. The lack of dilution near the centre indicates that there is no evidence for a featureless optical continuum produced by any ongoing non-stellar nuclear activity in this radio galaxy.

Our red spectra lack the resolution to obtain an accurate measurement of the equivalent width of the three lines of the Ca triplet. The equivalent width of the red line ($\lambda 8662$) can, however, be readily measured yielding $EQW(\lambda 8662) = 2.5\text{\AA}$ which is typical for a wide range of galaxy types (Terlevich et al., 1990).

3.5. The 2-micron emission

The K-band image (Fig. 2) which mainly represents the evolved stellar population is much more symmetrical about the central peak than the H α image which is dominated by the kpc-scale central disk. Even at this long wavelength where any obscuration due to dust must be small, we see no evidence for a nuclear concentration, though it might have been blurred due to the moderate seeing ($1.3''$). Another noteworthy feature is that Hydra A shows no sign of being perturbed by the elliptical neighbour seen 9 kpc southeast of the cD. This suggests that any gravitational interaction between the two galaxies must be minor, as also expected from the rather large radial velocity difference between them (630kms^{-1} ; see Heckman et al., 1985).

4. Discussion

4.1. Evidence for active star formation in the central disk

The detection of prominent and tilted Balmer absorption lines in the central region of Hydra A (Sect. 3.2) which is claimed to be located at the centre of a massive cooling flow may be specially relevant to the long-standing puzzle about the fate of the cooling gas (see the review by Fabian, 1994). Both the prominent Balmer absorption and the blue color of the central disk strongly suggest that the center of Hydra A has been the site of massive star formation activity over at least the past $\sim 10^7\text{yrs}$. Since tidal interaction of Hydra A with the neighbouring galaxy located 9 kpc to southeast seems unlikely (Sect. 3.5), the most plausible source of the material into the disk appears to be the cooling ICM of the surrounding cluster. The young stars in the central region, if massive enough, can provide an important source of ionizing radiation. This possibility is explored in following sections.

4.2. Energetics of the optical nebula

We now briefly examine some possibilities for powering the observed optical line emission from Hydra A with specific attention to the region within a radius $r_o = 2$ to 3 kpc where $\geq 80\%$ of the $H\alpha$ emission is concentrated. The $H\alpha$ luminosity emitted by this region is $\geq 6 \times 10^{40}$ erg s^{-1} corresponding to a total (bolometric) emission line luminosity $L_{bol} \sim 3 \times 10^{42}$ erg s^{-1} (see, Heckman et al., 1989). The cooling rate of the 4.5 keV gas within this region would be $\sim 5M_o/yr$, as inferred from the total cooling rate of $270M_o/yr$ and the known proportionality between radius and integral mass deposition rate within that radius (e.g., White & Sarazin, 1987). Assuming a temperature of $T_x = 10^8$ K the maximum thermal energy ($3/2nkT_x$) retrievable from the cooling gas is $\sim 10^{42}$ erg s^{-1} , barely enough to account for the optical luminosity of the nebula even assuming 100% conversion efficiency. A similar deficit has been noticed for several other putative cooling flow nebulae (see, Baum, 1992), motivating searches for additional sources of energy.

In a recent study Daines et al.(1994) have suggested that numerous cold cloudlets supported by the magnetic field are likely to accumulate within the inner region of cooling flows and dominate the dynamics in that region. The energy dissipated on this ensemble of (magnetized) cold cloudlets by the radio jets of Hydra A in the course of their precession (for which a period of $P \sim 3 \times 10^5$ yr has been inferred by modeling the observed wobbling of the jets. Taylor et al., 1990) can be estimated from the work done by jets on the cold material. Assuming conical geometry for the jets, this work is given by $(dE/dt)_j \sim \psi \rho_c (\pi \phi / P)^3 r_o^5$, where ψ is the opening angle, ϕ the angle of the precession cone, and ρ_c the density of the cold gas. For typical values of these parameters, $\psi = 0.1$ rad, $\phi = 0.1$ rad, and $\rho_c \sim 2-3$ times the density of hot gas (cf. Sect. 1) we estimate an energy deposition rate of $\sim 2 \times 10^{43}$ erg s^{-1} . Thus, the *stirring* of the inner nebula by the radio jets can perhaps be as important an energy source as the cooling ICM. Note that, even assuming an efficiency as high as 10% for the conversion of the jet's kinetic power into radio emission, the estimated power dissipation from the jets is only a minute fraction of their kinetic power which must be $\sim 10^{45}$ erg s^{-1} .

The discovery of massive young stars in the central region of Hydra A suggest that young stars can provide at least a fraction of the ionizing energy. About $7 \times 10^7 M_\odot$ are needed (for a Salpeter IMF with upper mass limit of $100 M_\odot$ and lower limit of $1 M_\odot$) to produce the observed blue luminosity if only $\sim 10\%$ of the light at $\lambda 3800\text{\AA}$ comes from the young burst. A burst of this strength will in turn produce a total ionizing luminosity of $L_{ion} \sim 2 \times 10^{43}$ erg s^{-1} at an age of 3×10^6 yr, $L_{ion} \sim 5 \times 10^{42}$ erg s^{-1} at an age of 10^7 yr, or $L_{ion} \sim 6 \times 10^{39}$ erg s^{-1} at an age of 3×10^7 yr (Leitherer & Heckman (1995)). Notice that this amount of mass in young stars is consistent with the expected mass deposition from the cooling gas inside the 3Kpc radius during $\sim 10^7$ yr.

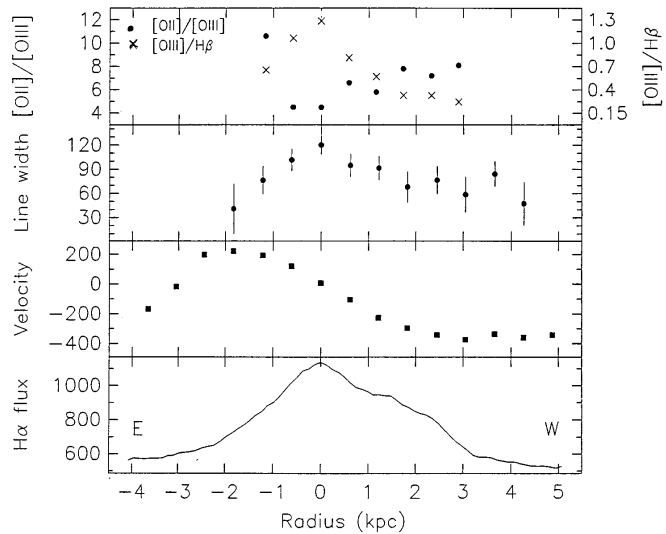


Fig. 10. Summary of the radial behaviour of some key parameters at PA = 102° . The lower three panels are based on the $H\alpha$ line profiles. The top panel depicts the spatial coincidence of the $H\alpha$ peak with the point of highest excitation level as inferred from two different line ratios. Note that the $H\alpha$ line width too attains the maximum at the $H\alpha$ peak.

4.3. Physical conditions and excitation of the gaseous disk

Fig. 10 summarizes the kinematical and photometric properties of the gaseous disk. A number of special locations can be noticed. Firstly is the nucleus where we find the maximum in both the line width and excitation level. The other special locations are the Western edge of the disk where we notice a local increase in the width of $H\alpha$ and a drop in the [SII] doublet ratio (no change in excitation), and the region immediately east of the nucleus where the excitation level drops sharply as indicated by the extremely large [OII]/[OIII] ratio. Note that this drop occurs well within the disk, far from the site where the rotation curve turns over which we identify as the edge of the disk.

It is thus evident that the spiral pattern visible in the disk corresponds to regions of higher excitation and higher velocity dispersion. The origin of these features appears therefore to be intimately linked to the excitation mechanism for the gas which we now discuss.

Heckman et al.(1989), have classified the emission line nebulae in cooling-flow clusters into two types according to their sizes, luminosities, and location in the line-ratio diagnostic diagrams. CF have presented a detailed study of three prominent cooling flow nebulae and suggest that rather than a dichotomy, there is a continuous range in the properties which can be parameterized in terms of the relative importance of the energy source for gas excitation: shocks produced by cloud-cloud collisions versus thermal energy of the hot ICM entrained in mixing layers on the surface of the cold clouds. Recall that Hydra A is a rather extreme class II nebula characterized by a large size, high luminosity, and weak [NII] and [SII] emission relative to $H\alpha$.

Fig. 9 presents a comparison of the observed line ratios with the values predicted by several representative models as indicated in the diagram. The rectangular boxes span the observed ranges for the different line ratios. These ratios have been corrected (to a first order) for the effect of underlying Balmer absorption as described in Sect. 3.3. Note that the scales are linear, and that the value of $[\text{OII}]/\text{H}\beta$ has been divided by 10 in order to fit within the same scale used for displaying the other line ratios.

As noted above, there is strong evidence for on-going massive star formation in Hydra A. The strength of the star-formation activity is large enough to provide more ionizing radiation than the cooling gas itself. Using the code CLOUDY we have estimated the emitted spectrum of a $3 \times 10^6 \text{ yr}$ old burst of star formation providing $2 \times 10^{43} \text{ erg s}^{-1}$ of ionizing radiation on top of the X-ray emission of the cooling flow. The young stars were represented by a 45,000K black-body. The X-ray emitted spectrum was assumed to be bremsstrahlung radiation by gas at a temperature $T = 5 \times 10^7 \text{ K}$. Constant density of gas (10^3 cm^{-3}) with solar composition was assumed. The resulting line ratios are plotted as solid squares in Fig. 9. It is clear that none of the models fit the entire set of observations. The poor fit of the shock models of Binette et al. (1985), to the $[\text{SII}]$ strengths is probably due to imprecise atomic parameters employed in these rather early models; the newer models of Sutherland et al. (1994) which use an improved version of the same code yield a better fit to the $[\text{SII}]$ lines (for similar abundances but lower pre-shock densities, however). The major caveat is that the models that fit the $[\text{OII}]$ and $[\text{OIII}]$ data do not fit the combination of the $[\text{NI}]$ and $[\text{OI}]$ measurements. The mixing-layer models of CF provide a poor fit to the strongest lines, but for extreme class II nebulae like Hydra A, CF predict that a significant fraction of the emission must be excited by shocks.

On the balance it seems that mixed Free-Free/young-stars models give a better fit to the observations of Hydra A nebula than pure mixing-layer and shock models. It remains to be seen whether data on the UV spectral lines quantitatively support this model.

4.4. Global geometry and morphology of the radio source

Under simple assumptions the observed shape of the $\text{H}\alpha$ disk can provide constraints on the orientation of the radio source. The disk appears to be roughly elliptical with an axial ratio of ~ 0.7 , elongated at $PA \sim 115^\circ$ which is nearly perpendicular to the radio jets ($PA \sim 20^\circ$, Taylor et al., 1990). Assuming the disk to be intrinsically circular, the apparent ellipticity would imply that its axis of symmetry is inclined by $\sim 45^\circ$ from the line-of-sight. This is very close to the inclination angle of the radio axis ($\sim 48^\circ$) deduced from modeling of the polarization observations of the radio lobes (Taylor & Perley, 1993). Note also that the modeling predicts that the northern part of the radio source lies on our side of the nucleus and is thus approaching us. This concurs with our detection of blue-shift of the nebular lines in the northern part, relative to the nucleus (Sect. 3.1).

An interesting clue as to the abrupt disruption of the radio jets may come from the observed fine structure of the $\text{H}\alpha$ nebulosity. Baum (1992) noted the possible presence of an ‘S’ shaped $\text{H}\alpha$ filament stretching all the way from the North to the South of the optical nebula (only the brighter northern part is discernible on our image; Fig. 1). It is tempting to speculate that interception of the radio jets by this extensive filament has led to their disruption which is evident from the VLA maps (Baum et al., 1988; Taylor et al., 1990). Additional evidence for a physical interaction between the northern jet and the filament comes from the presence of an $\text{H}\alpha$ hot spot at the putative point of impact (see, Fig. 1b of Baum, 1992) which also coincides with a peak in rotation measure (cf. Taylor & Perley, 1993). The trajectory of the southern filament needs to be better determined through deeper imaging before its possible role in the jet-flaring can be assessed.

5. Conclusions

In order to probe the structure, kinematics, stellar population, and energetics of the powerful nearby radio galaxy Hydra A we have performed slit-spectroscopy and $\text{H}\alpha$ imaging, supplemented with near-infrared imaging.

The $\text{H}\alpha$ image reveals structure of size $\sim 3 \text{ kpc}$ embedded within a central disk of ionized gas which dominates the $\text{H}\alpha$ nebulosity. We find the ionized gas to be rotating with a total velocity amplitude of $\geq 300 \text{ km s}^{-1}$. Our slit-spectroscopy reveals strong Balmer absorption lines in the near UV spectral range. This indicates the presence of O-B-A stars in the central $\sim 3 \text{ kpc}$. The Balmer absorption lines are tilted in a way that indicates a close kinematical coupling of the young stars and the rotating gaseous disk. On the other hand, the absorption lines characteristic of the old stellar population show no rotation. We argue that the disk is most likely associated with the cooling-flow of the X-ray emitting gas onto the center of the potential well of the galaxy and that the material could be ionized by the young stars and the X-ray from the cooling flow. The orientation of the disk perpendicular to the radio axis suggests a connection with the radio source.

The 2.2μ emission is found to have a much smoother and symmetric distribution than the $\text{H}\alpha$ emission. Thus, no major gravitational perturbation of the cD galaxy is evident.

Young stars appear to be potentially as relevant an energy source as the cooling intra-cluster medium for the excitation of the gas. No firm clues about the dominant excitation mechanism emerge from the emission-line ratios, although the combination of photoionization by young massive stars and free-free emission from the X-ray gas, gives a reasonable account of the observed optical line ratios.

Acknowledgements. We thank Patrice Bouchet for obtaining the IR image, Bo Reipurth for the $\text{H}\alpha$ image, Elena Terlevich for suggestions, Gary Ferland for the use of CLOUDY.

References

- Baum, S. A. 1992, in *Clusters and Superclusters of Galaxies*, ed., A. C. Fabian (Kluwer), p. 171
- Baum, S. A., Heckman, T. M., Bridle, A. H., van Breugel, W. J. M. & Miley, G. K. M. 1988, *ApJ Suppl*, 68, 643
- Bica, E., Alloin, D. & Schmitt, H.R. 1994, *A&A*, 283, 805
- Binette, L., Dopita, M. A. & Tuohy, I. R. 1985, *ApJ*, 297, 476
- Crawford, C. S. & Fabian, A. C. 1992, *MNRAS*, 259, 265 (CF)
- Crawford, C. S. & Fabian, A. C. 1993, *MNRAS*, 265, 431
- Daines, S.J., Fabian, A.C. & Thomas, P.A. 1994, *MNRAS* 268, 1060
- David, L. P., Arnaud, K. A., Forman, W. & Jones, C. 1990, *ApJ*, 356, 32
- Dressler, A. & Gunn, J. 1983, *ApJ* 270, 7
- Ekers, R. D. & Simkin, S. M. 1983, *ApJ*, 265, 85
- Fabian, A. C. 1994, *ARA&A* 32, 277
- Fanaroff, B. L. & Riley, J. M. 1974, *MNRAS*, 167, 31P
- Ford, H. et al. 1994, *ApJ (Letters)*, 435, L27
- Gopal-Krishna, Melnick, J., Giraud, E. & Steppe, H. 1992, *A&A*, 254, 42
- Goudfrooij, P., Norgaard-Nielsen, H. U., Hansen, L., Jorgensen, H. E., de Jong, T. 1990, *A&A*, 228, L9
- Hansen, L. 1989, in *Extranuclear Activity in Galaxies*, eds., E. J. A. Meurs & R. A. E. Fosbury, ESO (Garching), p.3
- Hansen, L., Jorgensen, H.E. & Norgaard-Nielsen, H.U. 1995, *A&A*, 297, 13
- Harnes, R. J. et al. 1994, *ApJ (Letters)*, 435, L35
- Heckman, T. M., Illingworth, G. D., Miley, G. K. & van Breugel, W. J. M. 1985, *ApJ*, 299, 41
- Heckman, T. M., Baum, S. A., van Breugel, W. J. M. & McCarthy, P. A. 1989, *ApJ*, 338, 48
- Jaffe, W., Ford, H., Ferrarese, L., van den Bosch, F. & O'Connell, R. W. O. 1993, *Nature*, 364, 213
- Jones, J.E., Alloin, D.M. & Jones, B.J.T. 1984, *ApJ* 283, 457
- Kato, T., Tabara, H., Inoue, M. & Aizu, K. 1987, *Nature*, 329, 223
- Maeder, A. & Chiosi, C. 1990
- Matthews, T.A., Morgan, W.W. & Schmidt, M. 1964, *ApJ*, 140, 35
- McNamara, B.R. 1995, *ApJ*, 443, 77
- Robinson, A. 1989, in *Extranuclear activity in Galaxies*, eds., E. J. A. Meurs & R. A. E. Fosbury, ESO (Garching), p. 259
- Sandage, A. 1973, *ApJ*, 183, 731
- Sandage, A. & Hardy, E. 1973, *ApJ*, 183, 743
- Simkin, S. M. 1979, *ApJ*, 234, 56
- Smith, E. P. & Heckman, T.M. 1989, *ApJ* 341, 658
- Sutherland, R.S., Bicknell, G. & Dopita, M.A. 1993, *ApJ* 414, 510
- Tabara, H., Kato, T., Inoue, M. & Ishiguro, M. 1990, *PASJ*, 42, L19
- Taylor, G. B. & Perley, R. A. 1993, *ApJ*, 416, 554
- Taylor, G. B., Perley, R. A., Inoue, M., Kato, T., Tabara, H., Aizu, K. 1990, *ApJ* 360, 41
- Terlevich, E., Diaz, A.I. & Terlevich, R. 1990, *MNRAS* 242, 271
- White, D.A., Fabian, A.C., Johnstone, R.M., Mushotzky, R.F. & Arnaud, K.A. 1991, *MNRAS* 252, 72
- White, R.E. & Sarazin, C.L. 1987, *ApJ* 318, 612